

We are IntechOpen, the world's leading publisher of Open Access books Built by scientists, for scientists

6,900

Open access books available

186,000

International authors and editors

200M

Downloads

Our authors are among the

154

Countries delivered to

TOP 1%

most cited scientists

12.2%

Contributors from top 500 universities



WEB OF SCIENCE™

Selection of our books indexed in the Book Citation Index
in Web of Science™ Core Collection (BKCI)

Interested in publishing with us?
Contact book.department@intechopen.com

Numbers displayed above are based on latest data collected.
For more information visit www.intechopen.com



Mechanical Properties Evaluation of Bulk and Coated Material by Depth Sensing Indentation

J.V. Fernandes¹, N.A. Sakharova¹, J.M. Antunes^{1,2} and M.C. Oliveira¹

¹CEMUC, Department of Mechanical Engineering,
University of Coimbra,

²Escola Superior de Tecnologia de Abrantes,
Instituto Politécnico de Tomar,

^{1,2}Portugal

1. Introduction

The mechanical characterization of materials represents an important domain of research into development. Tensile and hardness tests are generally used for such effect. Samples for tensile test require specific geometries and sizes, which often limits its use, in particular when the available amount of material is not enough to carry out the test, as in case of micro-components. The hardness test, by its simplistic and not destructive character, becomes desirable to its utilization in the evaluation of the mechanical properties of materials.

The conventional hardness test consists of the application of a load on an indenter. This penetrates the sample along the direction of the normal of its surface. The load applied acts during a preset time, after which is removed, making possible the measurement of the size of the residual indentation, through optic resources. This allows the determination of the hardness, defined as the ratio between the applied load and area of the residual indentation. The optical evaluation of the area of the residual indentation is limited, namely for very low applied loads and, consequently the resulting indentations have reduced dimension. However, during the last two decades, the development of the hardness equipments not only allowed to eliminate this limitation, but also to widen the application field of the hardness test. In fact, the advent of the Depth Sensing Indentation (DSI) equipments, making possible to plot the load - indentation depth curves, extended the application of the hardness test to scales close to the atomic one.

Moreover, the DSI equipments allow evaluating, not only the hardness, but also other mechanical properties, such as the Young's modulus (Doerner & Nix, 1986; Oliver & Pharr, 1992). Other mechanical properties, such as the yield stress and work-hardening coefficient (Dao et al., 2001; Antunes et al., 2007), of bulk and coated materials can be determined from the DSI results, by applying accurate models or inverse analysis procedures. Most of the achievements reached in this domain arise from the employment of numerical tools. For example, the possibility to carry out inverse analysis, i.e. to obtain the tensile curve of bulk and coatings materials, from the experimental load - indentation depth curve obtained by DSI, was possible due to the numerical simulation of the hardness test.

The aim of this chapter is to shed light on questions coupled with using of DSI tests for mechanical characterization of bulk and composite materials. In this context, this chapter reviews the reverse analysis procedures applied to experimental DSI results, with the aim to evaluate: (i) the stress – plastic strain curve of bulk materials; (ii) the Young's modulus of thin coatings; and (iii) the residual stress value of materials.

2. The depth – sensing indentation test

2.1 Load – indentation depth curves

The DSI equipments make possible to plot the load – indentation depth curve, also called indentation curve that represents the evolution of the applied load with the indentation depth, during the hardness test. This curve comprises a loading and an unloading part. In the meantime, a creep period can be carried on at the maximum load, which main purpose is to stabilize the deformation induced during loading. Also the accomplishment of a creep period is common during unloading, at the last or a relatively small load. This last creep period can be used for the purpose to correct the thermal drift of the equipment.

A schematic representation of the load – indentation depth curves of an elastic-plastic material is shown in Fig. 1. In this figure are indicated the maximum load applied, P_{max} , and the correspondent indentation depth, h_{max} ; h_f represents the indentation depth after unloading and h_c corresponds to the contact indentation depth at the maximum load, which allows to calculate the correspondent contact area, A_c (this value is equal to the area of the residual indentation, represented by the dimension a in the Fig. 1 (b)), which is necessary for the evaluation of the hardness and the Young's modulus.

In case of purely elastic materials, the loading and unloading parts of the indentation curves are coincident, and the residual indentation depth, h_f , is equal to zero. For materials with a rigid-plastic behaviour, both indentation depths, at the maximum load and after unloading, are equal ($h_f=h_{max}$); this is because there is not elastic recovery, during unloading.

2.2 Contact area

For the Vickers and Berkovich indenters (both have pyramidal geometry, with square and triangular bases, respectively), the most used indenters in DSI tests, the contact area for the ideal geometry is given by:

$$A_c = 24.5h_c^2 \quad (1)$$

where the contact indentation depth, h_c , is determined from the unloading part of the indentation curve, using the following equation (Oliver & Pharr, 1992):

$$h_c = h_{max} - h_s = h_{max} - \varepsilon CP_{max} \quad (2)$$

where C represents the compliance, i.e. the inverse of the stiffness, S , at the maximum load ($C = 1/S = (dh/dP)_{P_{max}}$) and ε is a parameter, depending on the indenter geometry, which defines the value of $h_s = \varepsilon CP_{max}$ (see Fig.1 (b)). The value of the geometrical parameter, ε , is between 0.72 and 1, depending on the indenter (see Fig. 1 (a)). For the Vickers and Berkovich indenters, ε is generally considered equal to 0.75 (Pharr & Bolshakov, 2002).

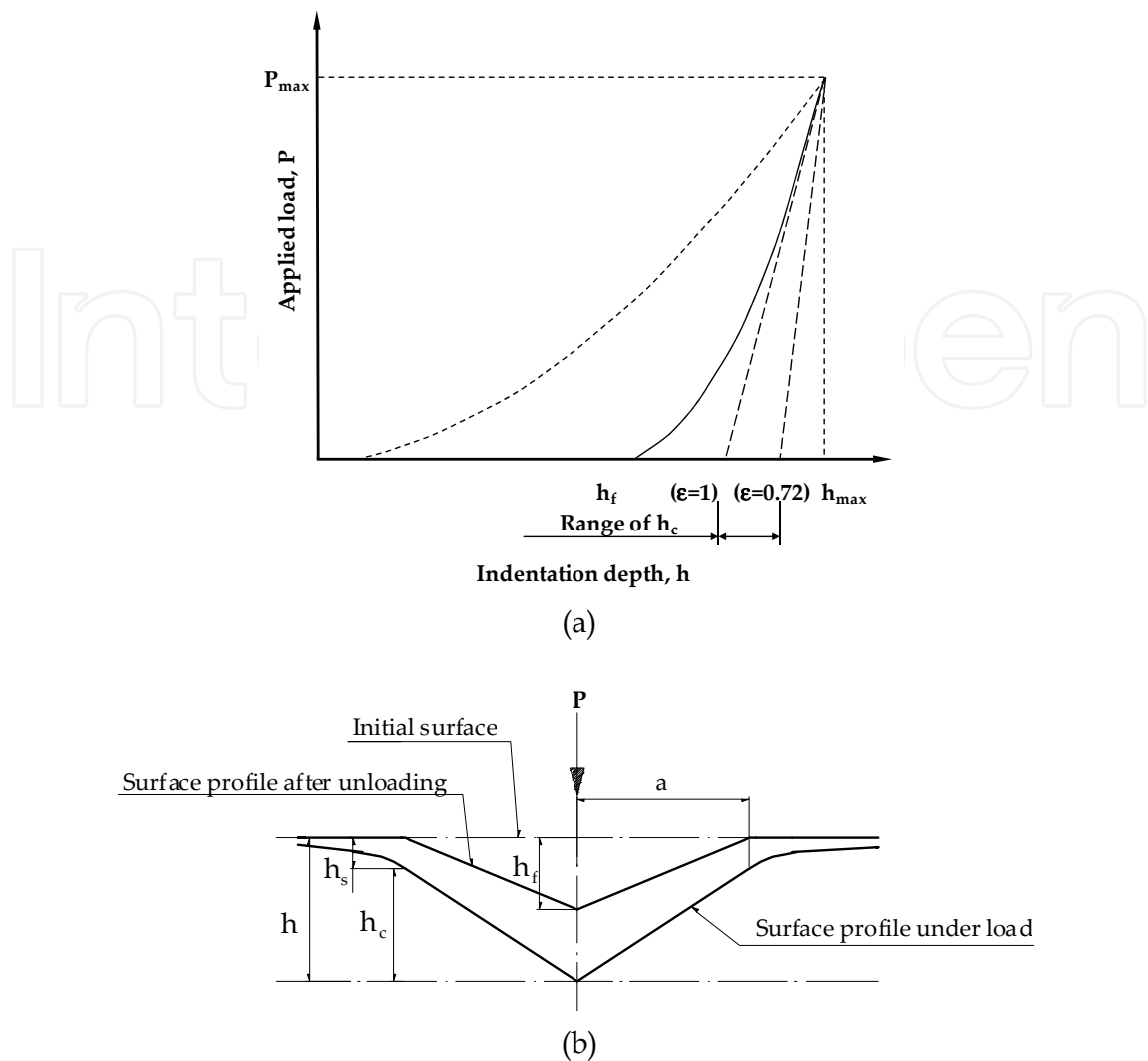


Fig. 1. Schematic representation of: (a) load – indentation depth curve (for simplicity, the creep periods are not shown); (b) correspondent geometrical parameters (Antunes et al., 2002).

2.3 Hardness and Young's modulus

The hardness, H_{IT} , is defined by the ratio between the maximum load and the contact area (ISO 14577, 2002):

$$H_{IT} = \frac{P_{\max}}{A_C} \quad (3)$$

It is also possible to determine the Young's modulus of the material from the indentation curve. Its evaluation is based on the Sneddon equation (Sneddon, 1965), which establishes a linear relationship between the applied load, P , and the elastic deflexion of the sample surface, h_e , indented by a rigid circular flat punch, with radius a :

$$P = \frac{2E}{(1-\nu^2)} ah_e \quad (4)$$

where E and ν are, respectively, the Young's modulus and the Poisson ratio of the material. From the above equation, it is possible to obtain: $dP/dh_e = 2Ea/(1-\nu^2)$. By making equivalence between a circular flat punch, acting on the surface of a material submitted to elastic deflection, and a pyramidal indenter, at the beginning of unloading, such that $A_c = \pi a^2$ and $(dh/dP)_{P_{\max}} = dh_e/dP$, it is possible to obtain an equation that relates the compliance at the maximum load, $C = (dh/dP)_{P_{\max}}$, with the reduced Young's modulus, E_r , for the case of a pyramidal indenter (ISO 14577, 2002):

$$C = C_0 + \frac{\sqrt{\pi}}{2E_r} \frac{1}{\sqrt{A_c}} \frac{1}{\beta} \quad (5)$$

C_0 and β , which are absent in Eq. (4), are included in this equation for taking into account: C_0 - the compliance of the equipment; and β - the differences of geometry between the circular flat punch and the pyramidal indenter. A recent review concerning the β value (Oliver & Pharr, 2004), suggests that its value is between 1.023 and 1.085. Moreover, the β value is higher for the Berkovich than for the Vickers indenter (for example: 1.05 for Vickers e 1.08 for Berkovich (Antunes et al., 2006)). The reduced Young's modulus, E_r , only depends on the elastic parameters of the tested material, if the indenter is considered rigid; however, in real cases, the reduced Young's modulus, E_r , depends also on the elastic parameters of the indenter:

$$\frac{1}{E_r} = \frac{(1-\nu^2)}{E} + \frac{(1-\nu_i^2)}{E_i} \quad (6)$$

where E and ν are, respectively, the Young's modulus and the Poisson ratio of the tested material (the reduced elastic modulus of the material is defined: $E^* = E/(1-\nu^2)$), E_i and ν_i are the correspondent elastic parameters of the material of the indenter. In case of diamond indenters (Vickers, Berkovich or conical): $E_i = 1140$ GPa and $\nu_i = 0.07$.

3. Plastic properties of bulk materials

The objective to use the hardness test for characterization of the materials, in order to relate its results with the tension behaviour retraces to years 20 of the past century. L. Prandtl (Prandtl, 1920) was the one of the pioneers in this area, when relating the hardness of the material with its resistance to the entrance in the plastic regimen, using the slip-line method, for the case of a flat punch. Afterward, a study concerning the indentation of ductile materials with resource to the spherical cavity model, allowed estimating a relationship between the hardness and the yield stress (Bishop & Mott, 1945). Based on hardness results performed in mild steel and copper, Tabor (Tabor, 1951) found a linear relationship between the hardness and the representative stress, σ_r (coupled with a value of plastic strain in tension, ϵ_r , i.e. the so-called representative plastic strain). This means that different materials with tensile curves crossing each other at the same point (σ_r, ϵ_r) show the same hardness value. The equation between the hardness and the representative stress was deduced based on former studies (Hill et al., 1947), and can be expressed (Tabor, 1951):

$$H_{IT} = \eta \sigma_r \quad (7)$$

where H_{IT} is the hardness, η is a parameter ($\eta=3.3$, for the Vickers indenter) and σ_r is the representative stress, corresponding to a representative plastic strain, ε_r , equal to 0.08. Also, based on previous studies (Bishop & Mott, 1945; Hill, 1950; Marsh, 1964; Hirst & Howse, 1969), K.L. Johnson (Johnson, 1970) proposed the following relationship between the hardness, H_{IT} , and the representative stress, σ_r , for elastic-plastic materials:

$$\frac{H_{IT}}{\sigma_r} = \frac{2}{3} \left[1 + \ln \left(\frac{E}{6\sigma_r(1-\nu)} \operatorname{tg}\alpha + \frac{2(1-2\nu)}{3(1-\nu)} \right) \right] \quad (8)$$

where E and ν are the Young's modulus and the Poisson ratio of the material, respectively, and α is the angle between the sample surface, normal to the loading axis, and the surface of the indenter. The representative stress, σ_r , is related to the representative plastic strain, ε_r , which depends on the apical indenter angle, $\phi=(\pi/2-\alpha)$, through the equation (Johnson, 1970):

$$\varepsilon_r = 0.2 \cot \phi \quad (9)$$

Subsequently, bi- and tri-dimensional numerical simulation results of the hardness test of several materials, using a conic indenter with an apical angle equal to 70.3° (for which the contact area is consistent with Eq. (1)), allow establishing dimensionless Π functions for characterizing the plastic behaviour (Dao et al., 2001). The Π functions allow establishing an inverse analysis procedure for determining the stress - plastic strain curve of materials, from the indentation curves.

The stress - plastic strain curve can be defined from the representative stress and strain and the work-hardening coefficient, n , when described by the Swift law (Swift, 1952):

$$\sigma = k(\varepsilon_0 + \varepsilon)^n \quad (10)$$

where σ and ε are the stress and the plastic deformation, respectively; n (work-hardening coefficient), k and ε_0 (which value is very low: close to $\varepsilon_0 = \sigma_0/E$, where σ_0 is the yield stress) are material constants. The knowledge of the pair $(\sigma_r, \varepsilon_r)$, ε_0 and n allows determining the constant k of the Swift law: $k = \sigma_r / (\varepsilon_0 + \varepsilon_r)^n$. The yield stress can be determined as: $\sigma_0 = k\varepsilon_0^n$.

For determining the representative stress, the following dimensionless function, Π_1 , was proposed (Dao et al., 2001):

$$\begin{aligned} \frac{K}{\sigma_r} = \Pi_1 \left(\frac{E^*}{\sigma_r} \right) = & -1.311 \left[\ln \left(\frac{E^*}{\sigma_r} \right) \right]^3 + 13.635 \left[\ln \left(\frac{E^*}{\sigma_r} \right) \right]^2 + \\ & + 30.549 \left[\ln \left(\frac{E^*}{\sigma_r} \right) \right] + 29.267 \end{aligned} \quad (11)$$

where K is the constant of the Kick law (Kick, 1885), which describes the loading part of the indentation curve (Kick law: $P = Kh^q$; in absence of indentation size effect, as in assumed by (Dao et al., 2001): $q=2$), and E_r is the reduced elastic modulus of the material ($E^* = E/(1-\nu^2)$).

In Eq. (11), the representative stress, σ_r , and the correspondent representative plastic deformation, $\varepsilon_r = 0.033$, concern materials with equal reduced elastic modulus and with tensile stress - plastic strain curves that cross each other at the same point $((\sigma_r, \varepsilon_r))$, even if with different values of the work-hardening coefficient. That is, the evolution of the ratio K/σ_r versus E^*/σ_r is independent of the work-hardening coefficient, for materials with the same representative stress, σ_r , corresponding to a representative plastic strain $\varepsilon_r = 0.033$, as shown in Fig.2. In case of $\varepsilon_r \neq 0.033$, Eq. (11) is not unique, i.e. the evolution of K/σ_r versus E^*/σ_r depends on the work-hardening coefficient of the material.

The full description of the tensile curve needs also the estimation of the work-hardening coefficient. From the knowledge of the values of the reduced elastic modulus ($E^* = E/(1-\nu^2)$) and the representative stress ($\sigma_r = \sigma_{0.033}$, corresponding to $\varepsilon_r = 0.033$) of the material, the work-hardening coefficient can be determined from one of the following functions, Π_2 or Π_3 (Dao et al., 2001) as it is given by Eqs. (12) and (13).

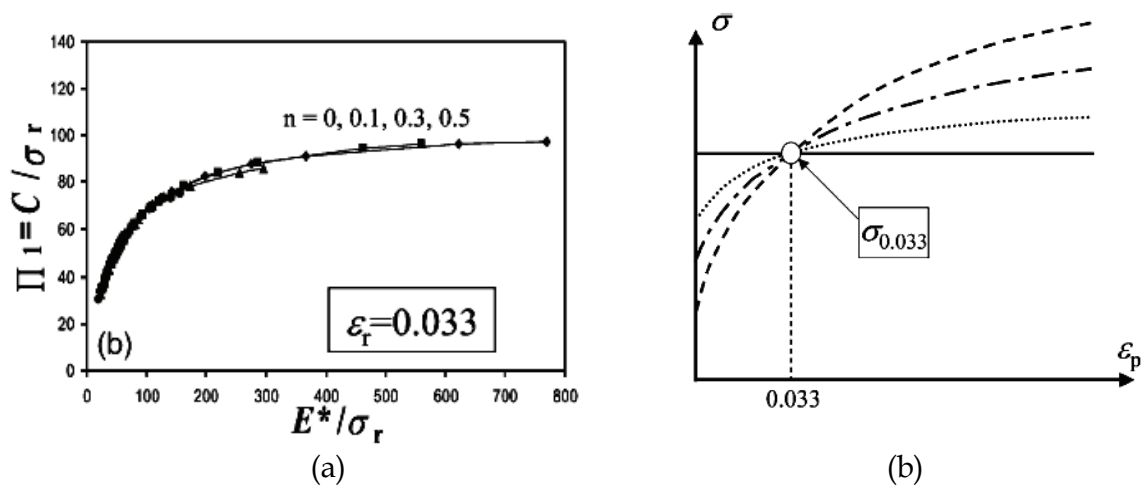


Fig. 2. Π_1 (Eq. (11)) versus E^*/σ_r (numerical results), for the case: $\varepsilon_r = 0.033$ (on the left). Tensile stress - plastic strain curves (on the right) (Dao et al., 2001).

$$\begin{aligned}
 \frac{1}{E^* h_{\max} C} = \Pi_2 \left(\frac{E^*}{\sigma_{0.033}}, n \right) &= (-1.40557n^3 + 0.77526n^2 \\
 &+ 0.15830n - 0.06831 \left[\ln \left(\frac{E^*}{\sigma_{0.033}} \right) \right]^3 + (17.93006n^3 \\
 &- 9.220911n^2 - 2.37733n + 0.86295) \left[\ln \left(\frac{E^*}{\sigma_{0.033}} \right) \right]^2 \\
 &+ (-79.99715n^3 + 40.556201n^2 + 9.00157n - 2.54543) \\
 &\left[\ln \left(\frac{E^*}{\sigma_{0.033}} \right) \right] + (122.65069n^3 - 63.884181n^2 - 9.58936n \\
 &+ 6.20045)
 \end{aligned} \tag{12}$$

$$\begin{aligned}
\frac{h_f}{h_{\max}} = \Pi_3 \left(\frac{E^*}{\sigma_{0.033}}, n \right) = & (0.010100n^2 + 0.0017639n \\
& -0.0040837) \left[\ln \left(\frac{E^*}{\sigma_{0.033}} \right) \right]^3 + (0.14386n^2 + 0.018153n \\
& -0.088198) \left[\ln \left(\frac{E^*}{\sigma_{0.033}} \right) \right]^2 + (0.59505n^2 + 0.034074n \\
& -0.65417) \left[\ln \left(\frac{E^*}{\sigma_{0.033}} \right) \right] + (0.58180n^2 - 0.088460n \\
& -0.67290)
\end{aligned} \tag{13}$$

where h_{\max} and h_f (see Fig. 1) are the indentation depths at the maximum load and after unloading, respectively, and C is the material compliance (in (Dao et al., 2001) it is used a rigid indenter in their simulations; so, in real cases, the compliance value, C , to be considered in this equation is $(C-C_0)$, i.e. the compliance simply due to the material).

However, this inverse analysis procedure has restrictions concerning the estimation of a unique solution for the work-hardening coefficient, namely in case of materials for which $\sigma_0/E_r \geq 0.033$ and $n \geq 0.3$ (σ_0 and n are the yield stress and the work-hardening coefficient of the material, respectively). In this case, for different n values the curves are quite close or even cross each other for low values of the ratio E^*/σ_r (Dao et al., 2001).

Other inverse analysis procedures were proposed, similar to the above mentioned (Dao et al., 2001), but making use of experimental indentation curves obtained using multiples indenters, with different values of the apical angle. The use of two or more indenter with different equivalent apical angles allows obtaining a unique solution for the work-hardening coefficient as in (Bucaille et al., 2003; Cao et al., 2005; Casals & Alcalá, 2005; Swaddiwudhipong et al., 2005), for example. The main difference between these procedures is the type of proposed functions. The inconvenience, common to all these procedures, is the experimental use of multiple indenters.

Recently, a new reverse analysis procedure, making use of results obtained with single indenter geometry, was proposed by (Antunes et al., 2007). The methodology, based on three-dimensional numerical simulations of the hardness test, is constructed in order to ensure unique results for the representative stress and the work-hardening coefficient. In a first step, it extracts the representative stress and plastic strain, which have a slight dependence on the elastic modulus, as shown in Fig.3.

This figure shows that for each value of the representative stress, the evolution of the associated plastic strain with the reduced Young's modulus is approximately linear, for values of this modulus below 450 GPa. In this case, the representative plastic strain slightly increases from a value close to 0.034, to values that depend on the representative stress, reaching a maximum of 0.042 when the representative stress is equal or higher than 3 GPa. For values of the reduced Young's modulus higher than 450 GPa, the representative plastic strain only depends on the representative stress of the material. In the second step, the hardening exponent is deduced from the unloading stiffness.

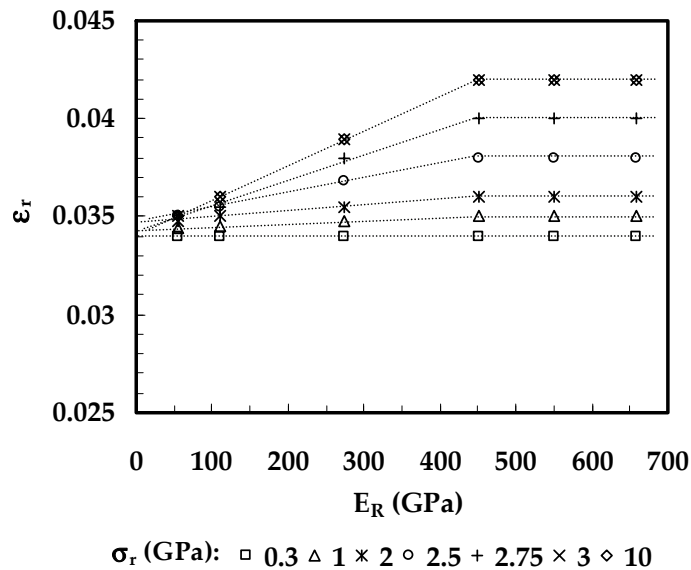


Fig. 3. Representative plastic strain, ϵ_r , versus the material reduced elastic modulus, E^* (in the figure E_R has the same meaning that E^*), for different values of the representative stress, σ_r (Antunes et al., 2007).

Concerning the first step, it was observed a quasi-linear relationship between E^*/H_{IT} and E^*/σ_r , independently on the work-hardening coefficient:

$$\frac{E^*}{H_{IT}} = 0.231 \left(\frac{E^*}{\sigma_r} \right) + 4.910 \quad (14)$$

The use of this equation, for estimation of the representative stress, σ_r , presume the previous experimental determination of the hardness, H_{IT} , and the reduced elastic modulus of the material, E^* , from the hardness test. The representative stress obtained by Eq. (14) can still be optimized by comparing the experimental and numerical indentation curves, by comparing the correspondent values of the maximum load P_{max}^{exp} (experimental maximum load) and P_{max}^{num} (numerical maximum load), obtained at the maximum indentation depth, h_{max} . In each iteration, the value of the representative stress used as input in the numerical tests, is altered until coincidence of the numerical curve with the experimental one is obtained, i.e. $P_{max}^{num} = P_{max}^{exp}$. A possible optimization strategy uses the ratio of the maximum loads, $P_{max}^{num}/P_{max}^{exp}$ to update the value of the representative stress:

$$\sigma_r(i+1) = \sigma_r(i) \left[\frac{P_{max}^{exp}}{P_{max}^{num}} \right] \quad (15)$$

where $\sigma_r(i+1)$ and $\sigma_r(i)$ are the (i+1) and (i) order values of the representative stress to be tested. The iterative process ends when the ratio between maximum loads approximates one, with the desired error.

Fig. 4 shows a numerical example of reverse analysis for determination of representative stress. The load-unloading curves, experimental and numerical, obtained during the optimization process of the representative stress, are shown. Apparently, all curves are

identical. The initial approximation of the representative stress (1st iteration), obtained with Eq. (14) was 0.227 GPa, which corresponds to an error in the maximum load of about 1%. Fig. 4b shows that, in the 3rd iteration of the stress optimization, identical values of maximum load (error less than 0.1%) for curves, experimental and numerical, were obtained (material with representative stress, $\sigma_r=0.229$ GPa)

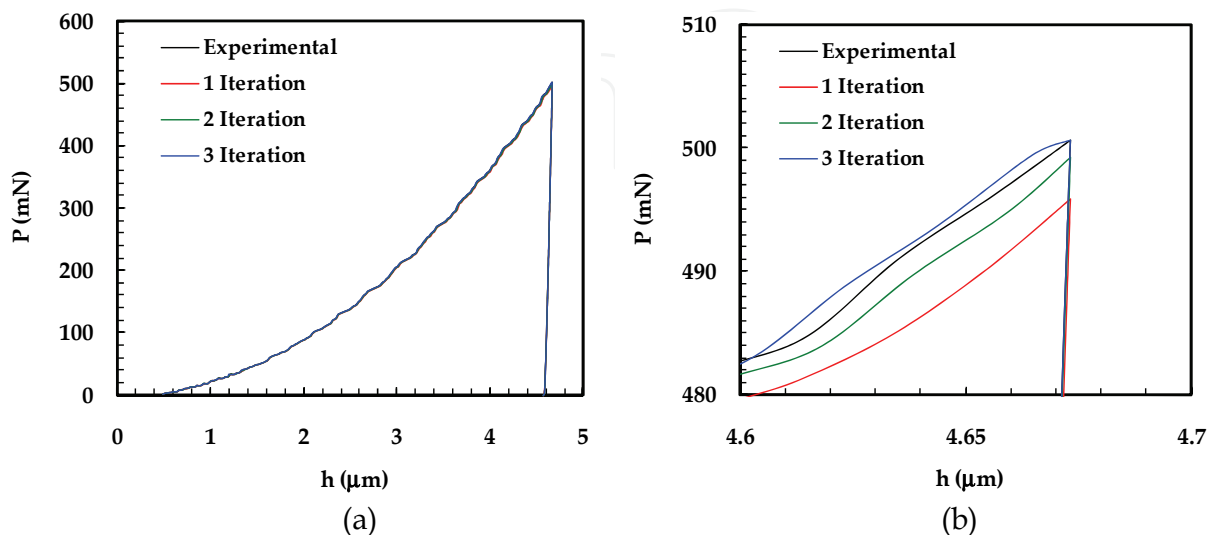


Fig. 4. Example of iterations, in order to make coincident the loading part of the indentation curves (Antunes et al., 2007): (a) full load-unloading curves; (b) detail of the region close to the maximum load.

Concerning the second step, for evaluating the work-hardening coefficient, this inverse analysis procedure requires the previous experimental determination of the stiffness, ($S = 1/C = (dP/dh)_{P_{\max}}$), determined from the unloading part of the indentation curve (in addition to the representative stress, determined in the first step). This stage of the inverse analysis consists on the comparison of the experimental S value, with the ones obtained by numerical simulation tests on materials, having the reduced elastic modulus, E^* , experimentally determined, as for the previous step, and the representative stress, σ_r , determined in the first step, but with different values of the work-hardening coefficient, n (Swift law (Eq. (10)), varying in a previously chosen range. Examples of numerical simulation results are shown in Fig. 5.

Fig. 6 shows that the unloading part of the indentation curve depends on the work-hardening coefficient, when the tensile curves cross each other at the same point (σ_r, ϵ_r) and the material has the same reduced elastic modulus. The most efficient way to compare the unloading part of the experimental and numerical indentation curves is using the value of the stiffness in the maximum load. So, the plotting of the stiffness, S^{num} , numerically obtained as a function of the work-hardening coefficient, n , allows the comparison with the experimental stiffness, S^{exp} , as shown in the example of Fig. 6. The evolution of S versus n follows, for the studied cases, a straight line, which makes easier the comparison between experimental and numerical results (two or three numerical simulations are enough for describing such linear behaviour). For the case of Fig. 6, the work-hardening coefficient of the material is close to 0.27.

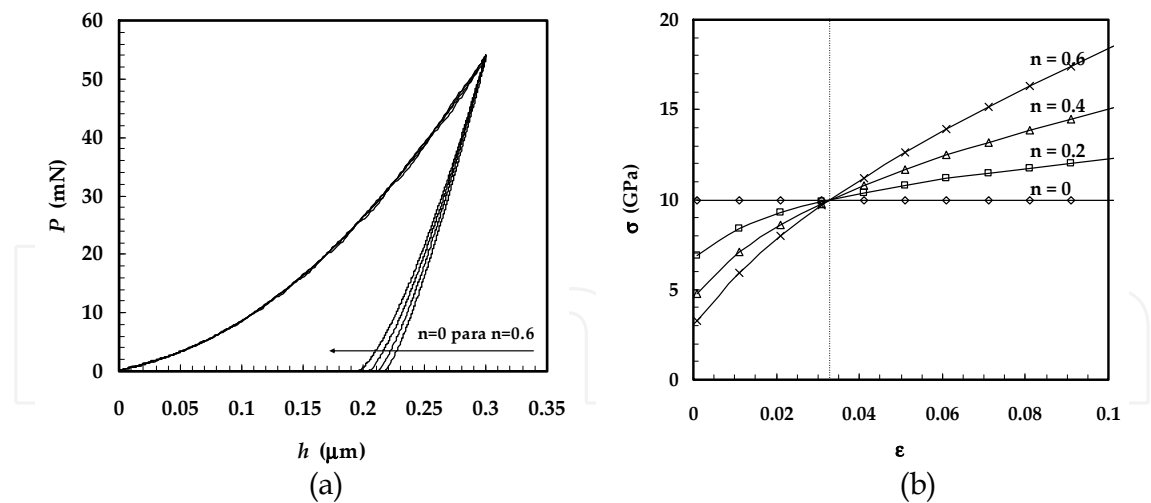


Fig. 5. (a) Examples of indentation curves obtained by numerical simulation of materials with the same reduced elastic modulus and stress - plastic strain curves crossing each other in the same point (σ_r, ϵ_r) ; (b) Schematic representation of correspondent stress - plastic strain curves, which only depend on the work-hardening coefficient (Antunes et al., 2007).

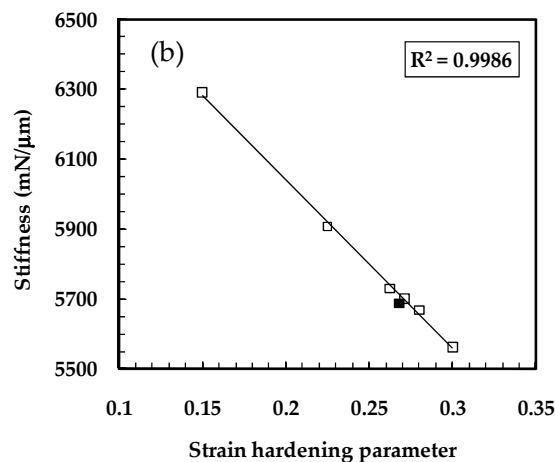


Fig. 6. Example of the evolution of the stiffness of the unloading indentation curve at the maximum load as a function of the work-hardening coefficient (open symbols: numerical results; solid symbol: experimental result) (Antunes et al., 2007).

When rigid indenters are used in the numerical simulations, the experimental and numerical stiffness values cannot be directly compared. In fact, in case of experimental unloading, the measured stiffness depends on the material and on the experimental equipment; in case of the numerical unloading, the stiffness depends only on the material. So, when using rigid indenters, previous to plot the experimental stiffness value on Fig. 6, an adjustment is required, in order to determined the equivalent value of the stiffness ($S_{\text{equi}} = 1/C_{\text{equi}}$). The equivalence between the compliance values, C_{equi} and C_{exp} , can be established by means of following equation (Antunes et al., 2007):

$$C_{\text{equi}} = \left(\sqrt{\frac{A_{\text{exp}}}{A_{\text{num}}}} \right) \left(C_{\text{exp}} - C_0 - \frac{1}{\beta} \frac{\sqrt{\pi}}{2} \frac{1}{\sqrt{A_{\text{exp}}}} \frac{(1-\nu_i)}{E_i} \right) \quad (16)$$

where C_0 is the compliance of the equipment, β is the correction factor of the indenter geometry, A_{exp} and A_{num} are the contact areas experimentally and numerically determined, respectively; ν_i and E_i are the Poisson's ratio and the Young's modulus of the experimental indenter, respectively.

4. Elastic modulus of thin coatings

The determination of the Young's modulus of thin coatings is significantly affected by the presence of the substrate. Indeed, the indentation region in elastic domain is not confined to the coating, but is extended to the substrate in particular for small thicknesses, almost from the beginning of the indentation. In this case, the determination of the Young's modulus is problematic, especially when there is a significant difference between the values of the modulus of the coating and of the substrate. The usual solution for this problem consists of separating the contribution of the thin coating from the composite Young's modulus results. In general, Young's modulus of thin coatings is extracted using analytical models (Doerner & Nix, 1986; King, 1987; Gao et al., 1992; Menčík et al., 1997; Saha & Nix, 2002; Antunes et al., 2007), which validity and restrictions seem to depend on the materials of the composite and on the test conditions.

Recently, a reverse analysis methodology, which allows avoiding the use of such analytical functions, for determination of the films' Young's modulus was proposed (Antunes et al., 2008). This methodology is based in a comparison of the composite Young's modulus, numerically evaluated by hardness tests, using a pyramidal indenter, with that obtained in the numerical simulation with flat punch indenters (with different areas), for the same values of equivalent relative contact indentation depth h/t (t is the thickness of the coating; in case of pyramidal indenter, h has the same meaning than h_c in Eqs. (1) and (2), in case of the flat punch indenter, the equivalent contact indentation depth $h = \sqrt{A}/24.5$, where A is the flat punch area). This comparison showed that the composite' Young's modulus results do not depend on the geometry of the indenter, but only on the contact area, as shown in Fig. 7.

The reverse analyses methodology consists on the experimental determination, by using a pyramidal indenter, of the contact area and of the reduced Young's modulus, E^* , for a given relative experimental contact indentation depth h/t . Subsequently, numerical simulations of the indentation test with a flat punch indenter are performed. For these simulations, the flat punch indenter must have the same equivalent relative contact area (or depth) that in case of the experimental test on the composite, with the pyramidal indenter; and the value of the substrate reduced Young's modulus is equal to the experimentally determined for the substrate, E_s^* which must be done previously. For the first simulation, a value for the films Young's modulus, $E_f^*(\text{punch})$, is chosen: $E_f^*(\text{punch})$ must be higher than E^* in case of $E^* > E_s^*$ or lower than E^* in case of $E^* < E_s^*$. The value of the composite Young's modulus, $E^*(\text{punch})$, numerically determined with the flat punch indenter is now compared with the one, E^* , experimentally determined with the pyramidal indenter. If the two values of the reduced modulus, $E^*(\text{punch})$ and E^* , are enough similar (within a predefined range of accuracy), then the reduced elastic modulus, E_f^* , can be estimated as being equal to $E^*(\text{punch})$. If there is a too great difference between the experimental (pyramidal) and numerical (flat punch) composite reduced elastic modulus (this is generally the case), then an iterative method will be used for optimization. This is, new values for $E_f^*(\text{punch})$ are chosen for numerical simulations with the flat punch indenter until the numerical and experimental values of the composite reduced modulus, $E^*(\text{punch})$ and E^* , are within the delimited range of accuracy.

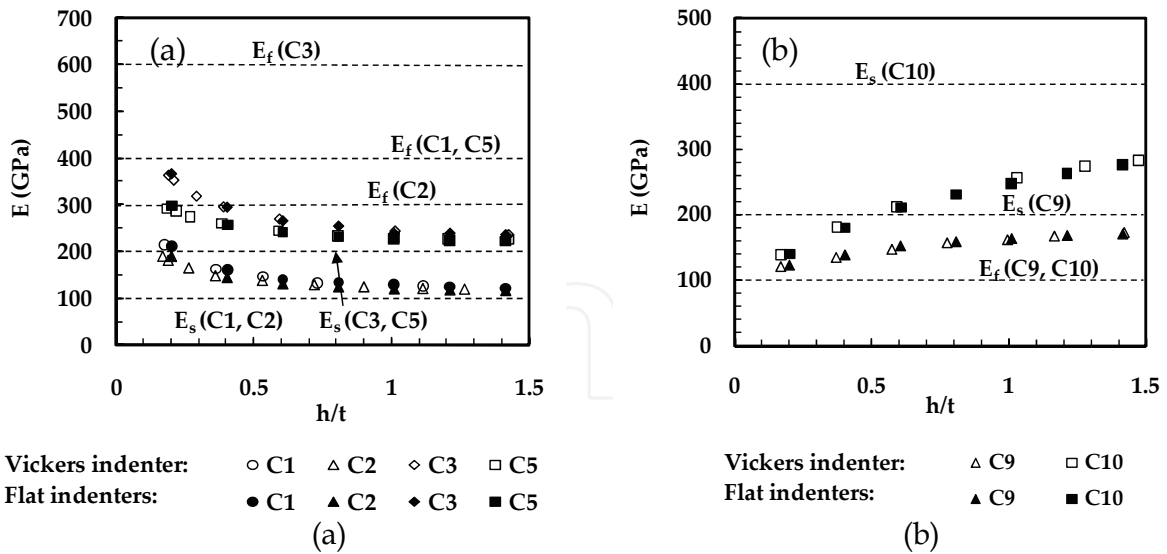


Fig. 7. (a) Composite Young's modulus, E , versus the normalized contact indentation depth, h/t (C1, C2, C3, C4, C5, C6, C7, C8, C9 and C10 concern composites with values of E_f/E_s of 4.00, 1.50, 3.00, 2.00, 2.00, 2.00, 1.00, 1.00, 0.50, 0.50, 0.25, respectively). Results obtained with Vickers and squared flat punch indenters (in this case the contact indentation depth is equal to the one of the Vickers indenter with the same contact area). (Antunes et al., 2007, 2008).

This inverse analysis methodology is accurate and easily performed. Moreover, the use of flat punch indenter ensures that no plastic deformation occurs in the composite, for small indentation depths, which excludes the requirement of knowledge the plastic properties of the film and the substrate, for performing the numerical simulations. In fact, the numerical simulation results of indentation tests with flat punch indenters show a linear relationship between the load, P , and the elastic deflexion of the sample surface, h_e , as described by Eq. 4 and shown in Fig. 8. This linear relationship allows us to calculate the elastic modulus of the composite, by using Eq. (4).

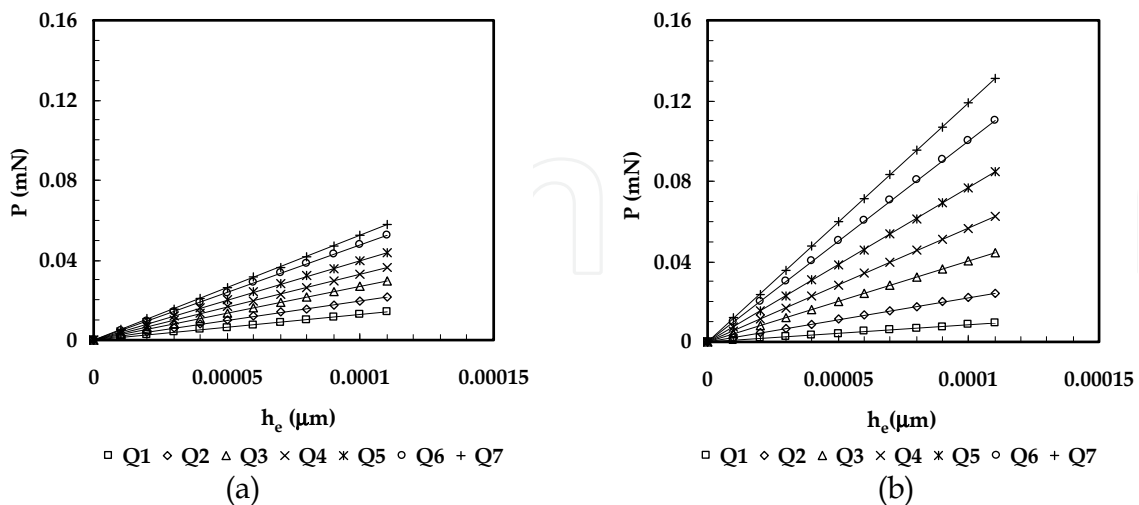


Fig. 8. (a) Load, P , versus the elastic deflexion of the sample surface, h_e , results obtained by numerical simulation, using squared flat punch indenters, with different areas (Q1: $0.25 \mu\text{m}^2$; Q2: $1.00 \mu\text{m}^2$; Q3: $2.25 \mu\text{m}^2$; Q4: $4.00 \mu\text{m}^2$; Q5: $6.25 \mu\text{m}^2$; Q6: $9.00 \mu\text{m}^2$; Q7: $12.25 \mu\text{m}^2$): (a) $E_f = 400$ GPa e $E_s = 100$ GPa; (b) $E_f = 100$ GPa e $E_s = 400$ GPa (Antunes et al., 2008).

5. Residual stresses

The evaluation of residual stresses is a topic of major interest for many engineering applications. In fact, the presence of surface residual stresses usually modifies the mechanical properties and performance of mechanical devices, such as the resistance to fatigue, fracture and corrosion (Golovin, 2008). For that reason, whereas compressive residual stresses are usually favorable and can even be intentionally induced to improve the mechanical properties, tensile residual stresses generally reduce the quality of performance, causing early failure of the products manufactured (Bocciarelli & Maier, 2007). Moreover, when the existence of residual stress is ignored, the measured mechanical properties do not correspond to the materials tested by the indentation (Golovin, 2008).

Several works have been performed in order to understand the effects of residual stresses on depth sensing indentation data, and procedures for extracting residual stresses have been proposed. It has been demonstrated that the indentation curve and thus the measured hardness depends on the residual stress level (Tsui et al., 1996; Bolshakov et al., 1996). Later, some other authors found similar results and proposed methodologies for extracting the residual stress (Suresh & Giannakopoulos, 1998; Chen et al., 2006) from depth sensing indentation data. Most of the times, these methodologies concern the case of in-plane surface equibiaxial residual stresses (although the case of uniaxial residual stress has also been studied; see for example (Zhao et al., 2006)) and consider the residual stresses uniform over the depth of influence of the indenter. A recent paper (Jang, 2009) critically reviewed and discussed issues and methodologies involved with residual stress estimation and its effects on depth sensing indentation results.

Important results characterize the influence of residual stress on the materials' mechanical properties determined by nanoindentation tests. The load-indentation depth curves obtained for samples subjected to compressive residual stresses are situated above the curve for material without residual stresses, and for samples subjected to tensile residual stresses the curves are positioned below the curve obtained for material without residual stresses. When the absolute value of residual stresses decreases, the load indentation curves tend towards the one obtained for material without residual stresses. Examples of load-indentation depth curves, obtained by numerical simulation of the nanohardness tests for materials subjected to different levels of compression and tension residual stresses are shown on Fig. 9 (Sakharova et al., 2011). Such behaviour is qualitatively representative for materials subjected to residual stresses and have been reported by various authors (Suresh & Giannakopoulos, 1998; Bocciarelli & Maier, 2007; Sakharova et al., 2011). The presence of residual stresses also affects the measured hardness: this hardness decreases for the samples with tensile residual stresses and increases for the samples with compressive residual stresses, although the influence of the residual stress is less important in compressive than in tension residual stress. Additionally, the maximum indentation load is sensitive to the residual stress value. A linear relationship was found between the relative maximum load $((P_r - P_{wr})/P_{wr})$, where P_r and P_{wr} are values of maximum load with and without residual stress, and the corresponding value of residual stress normalized by yield stress (σ_r/σ_0) , although the trend-lines have different slopes for each case in a given material (Sakharova et al., 2011).

Basing on these results, a reverse analysis methodology for the determination of sign and value of equibiaxial residual stresses in the surface of materials, from depth sensing indentation results obtained with pyramidal indenters, was very recently proposed (Sakharova et al., 2011). This reverse analysis methodology consists of obtaining coincidence between the loading part of numerical and experimental indentation curves for surface of

materials with residual stresses. The particularity of this approach is to rely exclusively on loading part of the indentation curve. In fact, the maximum load value is enough sensitive to detect the presence of residual stress, particularly in the cases of materials with low values of the E/σ_0 ratio.

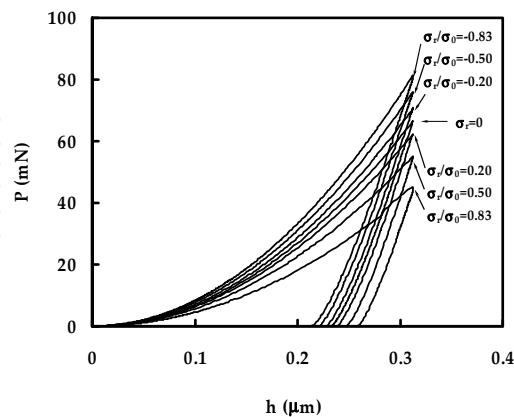


Fig. 9. Example of the load-indentation depth curves obtained with and without residual stresses of tension and compression for material with $E/\sigma_0 = 40$ (Sakharova et al., 2011).

The first step of this reverse analyses consists in carrying out experimental indentation tests up to a given value of maximum indentation depth, in two different regions of the sample: (i) a region with residual stress and (ii) a region far from the area subjected to residual stresses (on the edge of the sample, for example). The comparison of these curves permits the sign of residual stresses to be identified: tension or compression. For residual tension, the level of load-indentation depth curve obtained in region with residual stress is inferior to the one of the curve obtained in the region without residual stress; the opposite occurs for residual compression. In order to proceed with the reverse analyses, elastic (E and ν) and plastic (σ_0 and n) properties of the material are required, for input in numerical simulations. These properties can be determined independently (for example, by a tension test) or with an indentation test on a surface region without residual stresses, which permits both the elastic and plastic properties of the material to be determined, using the reverse analysis procedure as described in Section 3.

The next step, numerical simulations of indentation tests introducing different values of residual stresses in the programme must be carried out to estimate the residual stress value. Therefore, this reverse analysis methodology consists on the comparison of indentation curves: (i) numerically generated ones with residual stresses and (ii) experimental ones, both types obtained in regions of the sample with residual stresses. The best way to do this comparison is to build graphs, which show the evolution of residual stresses used as input in the numerical simulations, σ_{Nr} , as a function of the relative difference $(P_{Nr} - P_{expr})/P_{expr}$ between maximum loads obtained in the corresponding numerical test with residual stresses, P_{Nr} , and the one experimentally obtained in the region with residual stresses, P_{expr} . Three or four numerical tests can be sufficient, depending on the linear correlation obtained between σ_{Nr} , and $(P_{Nr} - P_{expr})/P_{expr}$.

Fig. 10. shows a schematic example of the determination of residual stress value. In this figure, the experimental load-indentation curves (with residual stresses) for the material chosen as example and the load-indentation depth curves obtained by numerical simulation for the same material with different level of σ_{Nr} (residual stress introduced in the numerical

simulations) as a function of relative difference, $(P_{Nr} - P_{expr}) / P_{expr}$, was built as shown in Fig. 10b. The interception of the linear trend-line with the vertical axis allows the value of residual stresses, σ_{Er} , to be estimated, since it occurs at the condition $P_{Nr} = P_{expr}$.

A real example of the determination of residual stress value is shown in Fig. 11a, for the case of equibiaxial compressive residual stress in commercial stainless steel SUS304-CSP specimens (Wang et al., 2006). The results obtained for the residual stress is $\sigma_{Er} = 618$ MPa (see Fig. 11a) very close to the mentioned by authors of (Wang et al., 2006), which was calculated by using their own method: $\sigma_{Er} = 631$ MPa.

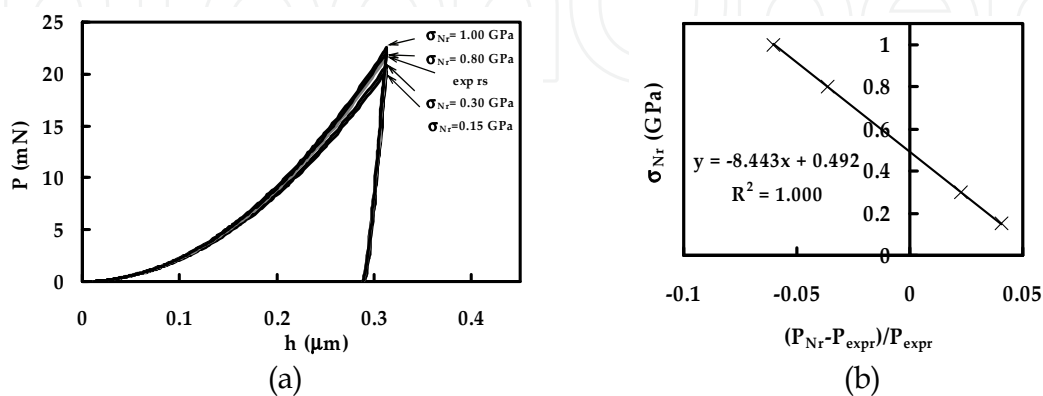


Fig. 10. (a) Load-indentation depth curves, obtained with residual stresses, experimental (exp rs) and numerically (σ_{Nr}) for material with $\sigma_0 = 1.50$ GPa, $n = 0.30$ and $E = 600$ GPa; (b) evolution of σ_{Nr} with the value of $((P_{Nr} - P_{expr}) / P_{expr})$, based on graph on (a), for the determination of σ_{Er} for this material (Sakharova et al., 2011); σ_r is the value of residual stresses considered; σ_{Er} - estimated residual stresses values obtained by inverse analysis.

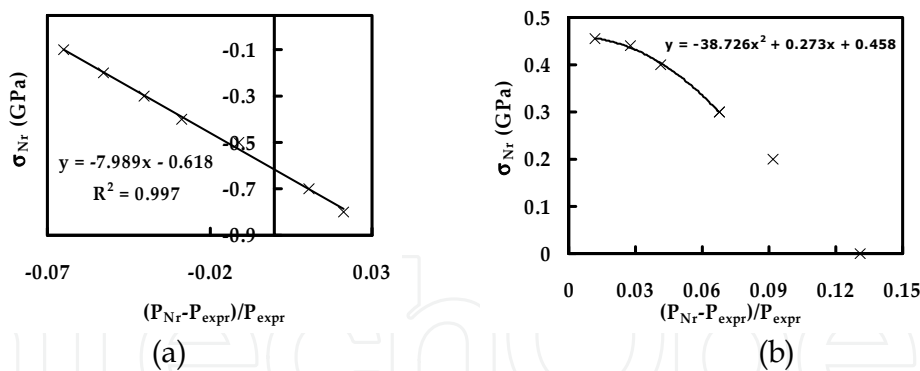


Fig. 11. Evolution of σ_{Nr} with the value of $((P_{Nr} - P_{expr}) / P_{expr})$ for the determination of σ_{Er} for (a) stainless steel SUS304-CSP specimens (Wang et al., 2006); (b) for API X65 steel plate specimens (Lee et al., 2004).

Furthermore, this reverse analysis procedure can be extended for indentation tests with any indenter geometry (Sakharova et al., 2011). In fact, this methodology was also successfully used for a non-pyramidal indenter, the Bralé indenter, for the case of equibiaxial tensile residual stress in small-grained API X65 steel plate specimens (Lee et al., 2004; Bocciarelli & Maier, 2007). In this case, the estimated mean value of residual stress is $\sigma_{Er} = 458$ MPa (considering the error of the experimental maximum load from the (Lee et al., 2004) results, the estimated residual stress value is in the range: 445 to 475 MPa), which is close to the experimentally determined by (Lee et al., 2004): $\sigma_{Er} = 440$ MPa.

It must be mentioned, that in Fig. 11b, where the results of the reverse analysis procedure are shown, a lack of linearity between σ_{Nr} and $(P_{Nr} - P_{exp r})/P_{exp r}$ occurred, probably due to the type of indenter geometry (Brale indenter instead of pyramidal indenter). For this reason, the extrapolation of σ_{Nr} for $(P_{Nr} - P_{exp r})/P_{exp r} = 0$, was carried out using a second degree polynomial equation.

6. Conclusion

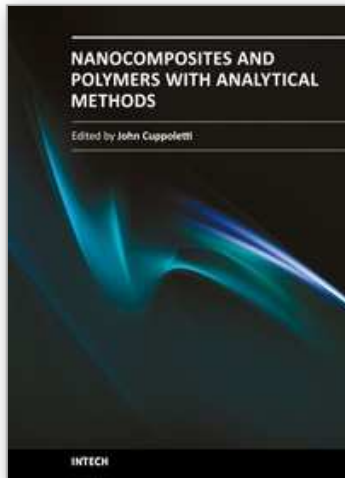
The mechanical characterization of materials represents an important domain of research into development. The hardness test, by its simplistic and not destructive character, becomes advantageous for utilization in the evaluation of the mechanical properties of materials. Depth Sensing Indentation (DSI) equipments, intensively developed during the last two decades, making possible to plot the load - indentation depth curves, extended the application of the hardness test to scales close to the atomic one. Moreover, the DSI equipments allow evaluating, not only the hardness, but also other mechanical properties, such as the Young's modulus. Other mechanical properties, such as the yield stress and work-hardening coefficient, of bulk and coated materials can be determined from the DSI results, by applying reverse analysis procedures. Most of the achievements reached in this domain arise from the employment of numerical tools. The examples mentioned in this review concern the option of carrying out reverse analysis, i.e. to obtain the tensile curve of bulk materials and the Young's modulus of thin coatings, from the experimental load - indentation depth curve obtained by DSI, with resource of numerical simulation of the hardness test. Also, numerical simulations of indentation tests are an important tool to determine the surface residual stresses, using only the loading part of the indentation curve to achieve the results. In generally, the above mentioned reverse analysis methodologies are simple, fast and accurate procedures for mechanical properties determination. Finally, it is important to note that no special software is needed to perform the numerical simulations of the hardness tests. A large number of commercial codes can be used with this objective.

7. References

- Antunes, J.M.; Cavaleiro, A.; Menezes, L.F., Simões, M.I. & Fernandes, J.V. (2002). Ultra-microhardness testing procedure with Vickers indenter, *Surface & Coatings Technology*, Vol. 149, No. 1, (1 January 2002), pp. 27-35, ISSN 0257-8972
- Antunes, J.M.; Menezes, L.F. & Fernandes, J.V. (2006). Three-dimensional numerical simulation of Vickers indentation tests, *International Journal of Solids and Structures*, Vol. 43, No. 3-4, (February 2006), pp. 784-806, ISSN 0020-7683
- Antunes, J.M.; Menezes, L.F. & Fernandes, J.V. (2007). On the determination of the Young's modulus of thin films using indentation tests, *International Journal of Solids and Structures*, Vol. 44, No. 25-26, (15 December 2007), pp. 8313-8334, ISSN 0020-7683
- Antunes, J.M.; Fernandes, J.V.; Sakharova, N.A. & Menezes L.F. (2008). Reverse analysis in depth-sensing indentation for evaluation of the Young's modulus of thin films, *Philosophical Magazine*, Vol. 88, No. 3, (21 January 2008), pp. 313-325, ISSN 1478-6435
- Bishop, R.F. & Mott, N.F. (1945). The theory of indentation and hardness tests, *Proceedings of the Physical Society of London*, Vol. 57, No. 321, pp. 147-159.
- Bocciarelli, M. & Maier, G. (2007). Indentation and imprint mapping method for identification of residual stresses, *Computational Materials Science*, Vol. 39, No.2, (April 2007), pp. 381-392, ISSN 0927-0256

- Bolshakov, A.; Oliver, W. C. & Pharr, G. M. (1996). Influences of stress on the measurement of mechanical properties using nanoindentation. 2. Finite element simulations, *Journal of Materials Research*, Vol. 11, No. 3, (March 1996), pp. 760-768, ISSN 0884-2914
- Bucaille, J.L.; Stauss, S.; Felder, E. & Michler, J. (2003). Determination of plastic properties of metals by instrumented indentation using different sharp indenters, *Acta Materialia*, Vol. 51, No. 6, (2 April 2003), pp. 1663-1678, ISSN 1359-6454
- Cao, Y.P.; Qian, X.Q.; Lu, J. & Yao, Z.H. (2005). An energy-based method to extract plastic properties of metal materials from conical indentation tests, *Journal of Materials Research*, Vol. 20, No. 5, (May 2005), pp. 1194-1206, ISSN 0884-2914
- Casals, O. & Alcalá, J. (2005). The duality in mechanical property extractions from Vickers and Berkovich instrumented indentation experiments, *Acta Materialia*, Vol. 53, No. 13, (August 2005), pp. 3545-3561, ISSN 1359-6454
- Chen X.; Yan J. & Karlsson, A. M. (2006). On determination of residual stress and mechanical properties by indentation, *Materials Science and Engineering: A*, Vol. 416, No. 1-2, (25 January 2006), pp. 139-149, ISSN 0921-5093
- Dao, M.; Chollacoop, N.; Van Vliet; K.J., Venkatesh, T.A. & Suresh, S. (2001). Computational modelling of the forward and reverse problems in instrumented sharp indentation, *Acta Materialia*, Vol. 49, No. 19, (November 2001), pp. 3899-3918, ISSN 1359-6454
- Doerner, M.F. & Nix, W.D. (1986). A method for interpreting the data from depth-sensing indentation instruments, *Journal of Materials Research*, Vol. 1, No.4, (April 1986), pp. 601-609, ISSN 0884-2914
- Gao, H.; Cheng-Hsin, C. & Jin, L. (1992). Elastic contact versus indentation modelling of multi-layered materials, *International Journal of Solids and Structures*, Vol. 29, No. 20, pp. 2471-2492, ISSN 0020-7683
- Golovin, Y.I. (2008). Nanoindentation and mechanical properties of solids in submicrovolumes, thin near-surface layers, and films: a review, *Physics of the Solid State*, Vol. 50, No. 12, (December 2008), pp. 2205-2236, ISSN 1063-7834
- Hill, R. (1950). *The mathematical theory of plasticity*, Clarendon Press, Oxford, United Kingdom
- Hirst, W. & Howse, M.G.J.W. (1969). Indentation of materials by wedges, *Proceedings of the Royal Society of London. Series A-Mathematical and Physical Sciences*, Vol. 311, No. 1506, pp. 429-444
- Hill, R.; Lee, E.H. & Tupper, S.J. (1947) The theory of wedge indentation of ductile materials, *Proceedings of the Royal Society of London. Series A-Mathematical and Physical Sciences*, Vol. 188, No. 1013, pp. 273-289
- ISO 14577 (2002). *Metallic materials – Instrumented indentation tests for hardness and materials parameters*, ISO Central Secretariat, Geneva, Suíça
- Jang, J. I. (2009). Estimation of residual stress by instrumented indentation: a review, *Journal of Ceramic Processing Research*, Vol. 10, No. 3, pp. 391-400, ISSN 1229-9162
- Johnson, K.L. (1970). The correlation of indentation experiments, *Journal of the Mechanics and Physics of Solids*, Vol. 18, No. 2, (April 1970), pp. 115-126, ISSN 0022-5096
- Kick, F. (1885). *Das Gesetz der proportionalen Widerstände und seine Anwendungen*, Felix-Verlag, Leipzig, German
- King, R.B., (1987). Elastic analysis of some punch problems for a layered medium, *International Journal of Solids and Structures*, Vol. 23, No. 12, (December 1987), pp. 1657-1664, ISSN 0020-7683
- Lee, Y. H.; Takashima, K.; Higo, Y. & Know, D. (2004). Prediction of stress directionality from pile-up morphology around remnant indentation, *Scripta Materialia*, Vol. 51, No. 9, (November 2004), pp. 887-891, ISSN 1359-6462

- Marsh, D.M. (1964). Plastic flow in glass, *Proceedings of the Royal Society of London. Series A-Mathematical and Physical Sciences*, Vol. 279, No. 137, pp. 420-435
- Menčík, J.; Munz, D.; Quandt, E.; Weppelmann, E.R. & Swain, M.V. (1997). Determination of elastic modulus of thin layers using nanoindentation, *Journal of Materials Research*, Vol. 12, No. 9, (September 1997), pp. 2475-2484, ISSN 0884-2914
- Oliver, W.C. & Pharr, G.M. (1992). An improved technique for determining hardness and elastic-modulus using load and displacement sensing indentation experiments, *Journal of Materials Research*, Vol. 7, No. 6, (June 1992), pp. 1564-1583, ISSN 0884-2914
- Oliver, W.C. & Pharr, G.M. (2004). Measurement of hardness and elastic modulus by instrumented indentation: Advances in understanding and refinements to methodology, *Journal of Materials Research*, Vol. 19, No. 1, (January 2004), pp. 3-20, ISSN 0884-2914
- Pharr, G.M. & Bolshakov, A. (2002). Understanding nanoindentation unloading curves, *Journal of Materials Research*, Vol.17, No. 10, (October 2002), pp. 2660-2671, ISSN 0884-2914
- Prandtl, L. (1920). Über die Harte plastischer Körper, *Nachrichten von der Königlichen Gesellschaft der Wissenschaften zu Göttingen: Mathematisch-physikalische Klasse*, Vol. 1920, (February 1920), pp. 74-85
- Sakharova, N. A.; Prates, P. A.; Oliveira, M. C.; Fernandes, J. V. & Antunes, J. M. (2011). A Simple Method for Estimation of Residual Stresses by Depth-Sensing Indentation, *Strain* (in press), online ISSN 1475-1305
- Saha, R. & Nix, W.D. (2002). Effects of the substrate on the determination of thin film mechanical properties by nanoindentation, *Acta Materialia*, Vol. 50 No. 1, (8 January 2002), pp. 23-38, ISSN 1359-6454
- Sneddon, I.N. (1965). The relation between load and penetration in the axisymmetric Boussinesq problem for a punch of arbitrary profile, *International Journal of Engineering and Science*, Vol 3, No. 1, (May 1965), pp. 47-57, 0020-7225
- Suresh, S. & Giannakopoulos, A. E. (1998). A new method for estimating residual stresses by instrumented sharp indentation, *Acta Materialia*, Vol. 46, No. 16, (9 October 1998), pp. 5755-5767, ISSN 1359-6454
- Swaddiwudhipong, S.; Tho, K.K.; Lui, Z.S. & Zeng, K. (2005). Material characterization based on dual indenters, *International Journal of Solids and Structures*, Vol. 42, No. 1, (January 2005), pp. 69-83, ISSN 0020-7683
- Swift, H.W. (1952). Plastic instability under plane stress, *Journal of the Mechanics and Physics of Solids*, Vol. 1, No. 1, (October 1952), pp. 1-18, ISSN 0022-5096
- Tabor, D. (1951). *The Hardness of Metals*, Clarendon Press, Oxford, United Kingdom
- Tsui, T. Y.; Oliver, W. C. & Pharr, G. M. (1996). Influences of stress on the measurement of mechanical properties using nanoindentation. 1. Experimental studies in an aluminum alloy, *Journal of Materials Research*, Vol. 11, No. 3, (March 1996), pp. 752-759, ISSN 0884-2914
- Wang, Q., Ozaki, K.; Ishikawa H.; Nakano, S. & Ogiso, H. (2006). Indentation method to measure the residual stress introduced by ion implantation, *Nuclear Instruments and Methods in Physics Research Section B: Beam Interactions with Materials and Atoms*, Vol. 242, No. 1-2, (January 2006), pp. 88-92, ISSN 0168-583X
- Zhao, M.; Chen, X.; Yan, J. & Karlsson, A. M. (2006). Determination of uniaxial residual stress and mechanical properties by instrumented indentation, *Acta Materialia*, Vol. 54, No. 10, (June 2006), pp. 2823-2832, ISSN 1359-6454



Nanocomposites and Polymers with Analytical Methods

Edited by Dr. John Cuppoletti

ISBN 978-953-307-352-1

Hard cover, 404 pages

Publisher InTech

Published online 09, August, 2011

Published in print edition August, 2011

This book contains 16 chapters. In the first part, there are 8 chapters describing new materials and analytic methods. These materials include chapters on gold nanoparticles and Sol-Gel metal oxides, nanocomposites with carbon nanotubes, methods of evaluation by depth sensing, and other methods. The second part contains 3 chapters featuring new materials with unique properties including optical non-linearities, new materials based on pulp fibers, and the properties of nano-filled polymers. The last part contains 5 chapters with applications of new materials for medical devices, anodes for lithium batteries, electroceramics, phase change materials and matrix active nanoparticles.

How to reference

In order to correctly reference this scholarly work, feel free to copy and paste the following:

J.V. Fernandes, N.A. Sakharova, J.M. Antunes and M.C. Oliveira (2011). Mechanical Properties Evaluation of Bulk and Coated Material by Depth Sensing Indentation, *Nanocomposites and Polymers with Analytical Methods*, Dr. John Cuppoletti (Ed.), ISBN: 978-953-307-352-1, InTech, Available from: <http://www.intechopen.com/books/nanocomposites-and-polymers-with-analytical-methods/mechanical-properties-evaluation-of-bulk-and-coated-material-by-depth-sensing-indentation>

INTECH
open science | open minds

InTech Europe

University Campus STeP Ri
Slavka Krautzeka 83/A
51000 Rijeka, Croatia
Phone: +385 (51) 770 447
Fax: +385 (51) 686 166
www.intechopen.com

InTech China

Unit 405, Office Block, Hotel Equatorial Shanghai
No.65, Yan An Road (West), Shanghai, 200040, China
中国上海市延安西路65号上海国际贵都大饭店办公楼405单元
Phone: +86-21-62489820
Fax: +86-21-62489821

© 2011 The Author(s). Licensee IntechOpen. This chapter is distributed under the terms of the [Creative Commons Attribution-NonCommercial-ShareAlike-3.0 License](#), which permits use, distribution and reproduction for non-commercial purposes, provided the original is properly cited and derivative works building on this content are distributed under the same license.

IntechOpen

IntechOpen